

Spiked Laplacian Graphs: Bayesian Community Detection in Heterogeneous Networks

Leo L. Duan ^{*}, George Michailidis [†], Mingzhou Ding [‡]

Abstract

In the network data analysis, it is common to encounter a large population of graphs: each has a small-to-moderate number of nodes but together, they show substantial variation from one graph to another. The graph Laplacian, a linear transform of the adjacency matrix, is routinely used in community detection algorithms; however, it is limited to single graph analysis and lacks uncertainty quantification. In this article, we propose a generative graph model called ‘Spiked Laplacian Graph’. Viewing each graph as a transform of the degree and Laplacian, we model the Laplacian eigenvalues as an increasing sequence followed by repeats of a flat constant. It effectively reduces the number of parameters in the eigenvectors and allows us to exploit the spectral graph theory for optimal graph partitioning. The signs in these orthonormal eigenvectors encode a hierarchical community structure, eliminating the need for iterative clustering algorithms. The estimator on the communities inherits the randomness from the posterior of eigenvectors. This spectral structure is amenable to a Bayesian non-parametric treatment that tackles heterogeneity. Theory is established on the trade-off between model resolution and accuracy, as well as the posterior consistency. We illustrate the performance in a brain network study related to working memory.

^{*}Department of Statistics, University of Florida, Gainesville, FL, email: li.duan@ufl.edu

[†]Department of Statistics & University of Florida Informatics Institute, University of Florida, Gainesville, FL, email: gmichail@ufl.edu

[‡]J. Crayton Pruitt Family Department of Biomedical Engineering, University of Florida, Gainesville, FL, email: mding@bme.ufl.edu

Keywords: Hierarchical Community Detection, Isoperimetric Constant, Mixed-Effect Eigendecomposition, Normalized Graph Cut, Stiefel Manifold

1 Introduction

In recent years, there has been a tremendous amount of interest in modeling network data. A particular focus has been on a single graph, with a large number of nodes that could grow indefinitely. For example, the stochastic block model (Karrer and Newman, 2011) and mixed membership stochastic block model (Airoldi et al., 2008) are very popular in analyzing social network with millions of users.

Another equally important scenario that receives much less attention is having a population of graphs, each with a small-to-moderate number of nodes. Most notably, typically in neuroscience, there is a large sample of brain networks, but each has only at most a few hundred regions of interests (Shen et al., 2013). As a result, the asymptotic result for the large graph is not suitable, as the uncertainty cannot be ignored. This has motivated various Bayesian graph models. Generally speaking, most of these methods can be viewed as some variants of the latent space model (Hoff et al., 2002), where the key idea is to assume a latent coordinate for each node, and the pairwise interaction of two coordinates (e.g., inner product, distance) determines the probability of whether an edge should form. Among others, Bayesian stochastic block model (van der Pas et al., 2018; Geng et al., 2019) characterizes the randomness in the community labels; some considers edge formation as a stochastic process, inducing properties such as power-law degree distribution (Cai et al., 2016), sparsity (Caron and Fox, 2017), link predictiveness (Williamson, 2016). Despite the recent flourish of Bayesian graph models, they tend to focus on the flexible modeling of a single small/large graph; there is arguably a lack of study on how well the single-graph generative model can generalize to multiple graphs, particularly if the graphs are not identically distributed.

Indeed, heterogeneity is a major challenge. The high variation from one graph to another makes it error-prone to pool information under a shared latent space. We are not the first to recognize this issue. To address this issue, Durante et al. (2017) proposed to use multiple sets of latent coordinates, modeled by a non-parametric mixture distribution. It achieves a much better fit to the data, compared to a naive averaging over multiple graphs. Similarly, Mukherjee et al. (2017) proposed an approach to directly cluster the graphs, which reduces the heterogeneity for downstream analysis in each group. We are inspired by the early work, but our focus is different: we are particularly interested in estimating the community structures and the distribution in the estimator; and we want to characterize the nuances among graphs.

The focus on community detection leads us to one of the most popular toolboxes in graph partition, the graph Laplacian (Chung and Graham, 1997). As a linear transform of the adjacency matrix, it plays a fundamental role in the spectral graph theory: its first few eigenvalues give a bound on the minimum edge loss when partitioning the graph into multiple sub-graphs, with each sub-graph as a community; using the eigenvectors, one can obtain a nearly optimal partitioning, also famously known as the spectral clustering. On the other hand, existing uses of Laplacian are highly algorithmic and involve multi-stage estimation, such as row normalization, singular value decomposition, rank-truncation, K-means (Ng et al., 2002); there is no likelihood associated with this, making it difficult for uncertainty quantification, let alone accommodating heterogeneity.

This motivates us to consider a generative model for the Laplacian, taking advantage of its spectral property while introducing non-parametric Bayes treatment on a population of graphs. The crux of the problem is how to parameterize a valid Laplacian but only focusing on the first few ranks? We borrow the idea from the unique structure of the

spiked covariance (Donoho et al., 2018), adding a new transformation so that we keep the few smallest eigenvalues (as opposed to the largest ones in covariance modeling). We then show that the associated eigenvectors contain useful information for a hierarchical bi-partitioning of the graph, which leads to an almost instantaneous estimation of the communities in each graph, with no need for iterative clustering algorithm like K-means. As a Bayesian model, the estimated community labels have a posterior distribution, which quantifies the uncertainty.

2 Method

Assuming we have a sample of S graphs, each denoted by $G^{(s)} = \{V, E^{(s)}\}$ with $s = 1, \dots, S$. They share the same set of nodes $V = \{1, \dots, n\}$, but individual set of edges $E^{(s)} = \{e_{i,j}^{(s)}\}_{i,j}$. Without loss of generality, we assume the edges are weighted and can be represented by an adjacency matrix $A^{(s)} = \{A_{i,j}^{(s)}\}_{i,j}$ with $A_{i,j}^{(s)} \geq 0$. For simplicity, we will focus on symmetric graph such that $A_{j,i}^{(s)} = A_{i,j}^{(s)}$ and with the diagonal $A_{i,i}^{(s)} = 0$.

2.1 Spiked Laplacian Graph

In this section, we will first introduce the generative model for one graph, and we omit the graph index (s) for concise notations. The normalized Laplacian is a linear transform of the adjacency matrix

$$L = D^{-1/2}(D - A)D^{-1/2}, \quad (1)$$

where $D = \text{diag}\{d_i\}_{i=1}^n$ the degree matrix, with $d_i = \sum_{j=1}^n A_{i,j}$. Equivalently, the adjacency can be written as a transform based on D and L , and from a generative process

$$\begin{aligned} D &\sim \Pi(D; \beta_D), \\ L &\sim \Pi(L; \beta_L), \\ A &= D^{1/2}(I_n - L)D^{1/2}, \end{aligned} \tag{2}$$

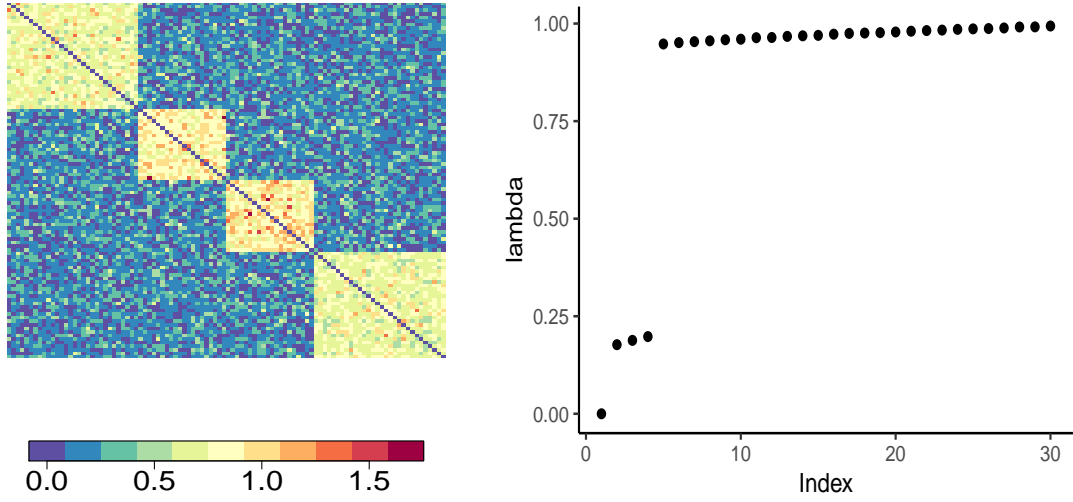
where we call $\Pi(D; \beta_D)$ the degree distribution and $\Pi(L; \beta_L)$ the Laplacian distribution, and we assume those two are independent. There are many choices when specifying $\Pi(D; \beta_D)$, such as the exponential random graph model (Robins et al., 2007); nevertheless, note that D does not contain much of the pairwise information, and most of the existing methods only need L for estimating the communities (Ng et al., 2002). Therefore, we consider D as ancillary and will focus on modeling $\Pi(L; \beta_L)$ from now on.

To assign $\Pi(L; \beta_L)$, we propose a structure for L

$$L = \mu_L + \mathcal{E}, \quad \mu_L = \sum_{k=1}^K \lambda_k q_k q_k^T + \sum_{l=K+1}^n \theta_l q_l q_l^T, \tag{3}$$

where \mathcal{E} is a symmetric matrix representing the noise, $\mathcal{E} = \{e_{i,j}\}_{i,j}$, $e_{i,j} \sim \text{No}(0, \sigma_e^2)$ for $i < j$; $e_{i,i} \sim \text{No}(0, 2\sigma_e^2)$ for a convenient matrix form (Hoff, 2009).

The matrix μ_L is symmetric and has eigenvalues $\lambda_1, \dots, \lambda_K, \underbrace{\theta, \dots, \theta}_{(n-K)}$ and eigenvectors q_1, \dots, q_n ; q_1, \dots, q_n are orthonormal. As a known property, the smallest eigenvalue of any Laplacian is always zero; hence we fix $\lambda_1 = 0$ and $q_1 = (1/\sqrt{n}, \dots, 1/\sqrt{n})$ (with the values justified later in Section 2.4). We call μ_L a ‘Spiked Laplacian’, with the name inspired by the spiked covariance (Donoho et al., 2018). The difference is that the spiked covariance sets the small eigenvalues to a constant; here, we set the large ones to a constant.



(a) Adjacency of a 4-community graph. (b) Eigenvalues of the normalized Laplacian L .

Figure 1: Plot of the eigenvalues from a normalized Laplacian: most of the eigenvalues are close to a constant, except with the first few close to 0. This motivates us to consider a model with spiked structure.

One intuition is that L is based on $-A$ as shown in (1); hence flattening the larger eigenvalues in $\mu_L = \mathbb{E}L$ is roughly doing the same for smaller ones in $\mathbb{E}A$. To show more motivation, we simulate a graph containing four communities, with relatively low connectivity across communities [Figure 1(a)]; then we compute its normalized Laplacian L and plot its raw eigenvalues in Figure 1(b). Note there are exactly four small eigenvalues, while the rest are close to a larger constant.

Having the spiked structure in μ_L not only reduces the number of parameters for the eigenvalues, but also for the eigenvectors. Using matrix notation $Q = (q_1, \dots, q_K)$, $\Lambda =$

$\text{diag}(\lambda_1, \dots, \lambda_K)$, we have an equivalent form

$$\mu_L = Q(\Lambda - I_K\theta)Q^T + I_n\theta, \quad (4)$$

notice that $(n - K)$ eigenvectors $\{q_l\}_{l=(K+1), \dots, n}$ are canceled in this alternative form, thus no longer need to be parameterize; we have $Q \in \mathcal{V}^{k \times n}$, a Stiefel manifold.

Thus far, we do not consider μ_L as generated given the community labels $c_i \in \mathbb{Z}^+$ for $i = 1, \dots, n$. This is because there is not a clear choice for the mixture distribution on the rows of Q , which can result in complicated computation due to the Stiefel constraints. Rather, we consider (c_1, \dots, c_n) as a fast transform based on (Q, Λ) , using a graph partitioning algorithm supported by the spectral graph theory. As shown later, this enjoys the advantages of hierarchical community detection, such as the adaptiveness to different community numbers for multiple graphs. On the other hand, although (c_1, \dots, c_n) is deterministic given the values of (Q, Λ) , since (Q, Λ) are random, we can obtain the posterior distribution $\Pi\{(c_1, \dots, c_n) \mid L\}$ by transforming $\Pi\{Q, \Lambda \mid L\}$, allowing uncertainty quantification.

2.2 Modeling Multiple Laplacians

To accommodate heterogeneity while borrowing information across graphs, we consider a ‘mixed-effects’ strategy: we treat $Q^{(s)}$ as the fixed effects, assuming there are only a few unique values among $\{Q^{(1)}, \dots, Q^{(S)}\}$; while we treat $\Lambda^{(s)}$ and $\theta^{(s)}$ as the random effects

for each s and allow flexible coefficient in each graph. For $s = 1, \dots, S$,

$$Q^{(s)} \sim \sum_{l=1}^{\infty} \pi_l \delta_{U^{(l)}}(\cdot), \quad \Pi(U^{(l)}) = \frac{\text{etr} \left[\Omega M^T U^{(l)} \right]}{{}_0F_1(\frac{1}{2}K, \frac{1}{4}\Omega\Omega)};$$

for $k = 2, \dots, K$:

$$\eta_k^{(s)} \sim \text{Bernoulli}(w), \quad \lambda_k^{(s)} \mid \eta_k^{(s)} = 0 \sim \text{No}_{(0,2)}(0, \sigma_{\lambda,0}^2), \quad \lambda_k^{(s)} \mid \eta_k^{(s)} = 1 \sim \text{No}_{(0,2)}(\mu_{\theta}, \sigma_{\lambda,1}^2),$$

$$\theta^{(s)} \sim \text{No}_{(0,2)}(\mu_{\theta}, \sigma_{\theta}^2).$$

(5)

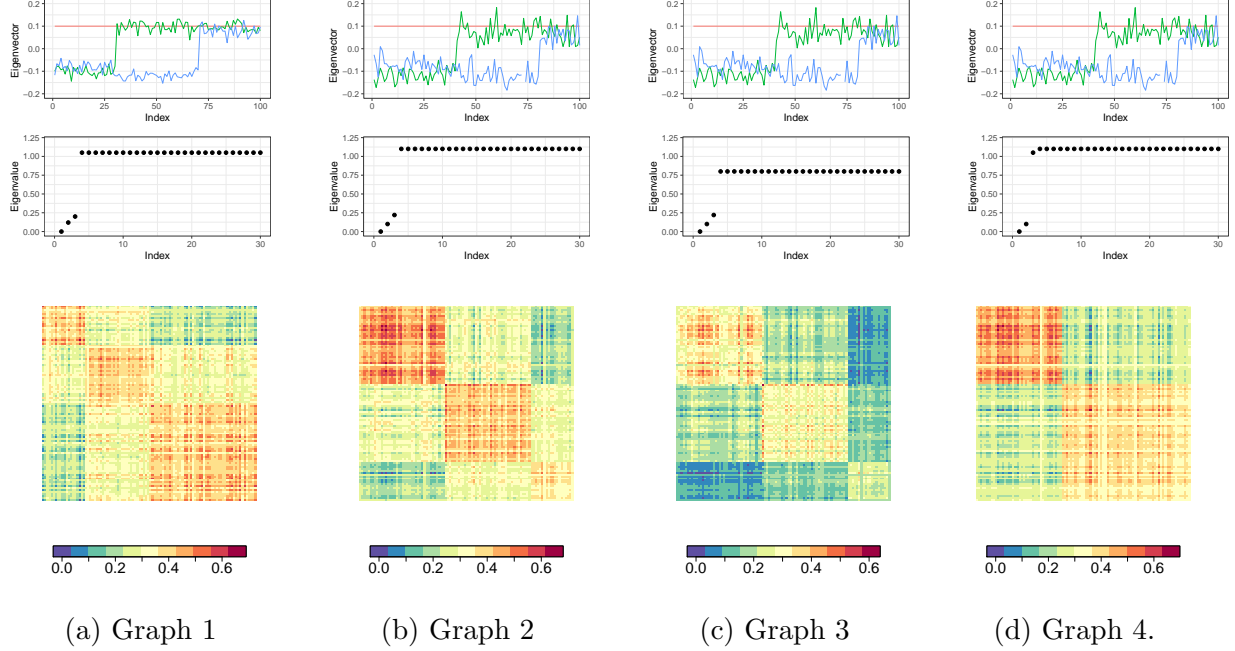


Figure 2: Illustration of how our model accommodates heterogeneity: Graphs 1 and 2,3,4 use two different eigen-matrices $Q^{(s)}$ (first row, first three eigenvectors shown), hence showing two distinct community structures in the adjacency matrices (third row). Graphs 2 and 3 have the both $\lambda_2^{(s)}, \lambda_3^{(s)} \approx 0$ (second row), showing three communities but of nuance in sparsity levels; Graph 4 only has $\lambda_2^{(s)} \approx 0$, showing only two clear communities.

The distribution for $Q^{(s)}$ is based on a stick-breaking process with base measure from a matrix Langevin distribution; $\pi_l = \nu_l \prod_{l' < l} (1 - \nu_{l'})$, $\nu_l \sim \text{Beta}(1, \alpha_0)$ and $\alpha_0 > 0$ the concentration parameter; $\delta_x(\cdot)$ is a Dirac measure at x ; M is a $n \times K$ matrix, Ω is an $K \times K$ diagonal matrix; ${}_0F_1$ is a hypergeometric function with matrix argument (Koev and Edelman, 2006). As the posterior of $Q^{(s)}$ will be atomic almost surely, it has a clustering effect that groups similar graphs together, with each component represented by $U^{(l)}$ such that $U^{(l)\text{T}}U^{(l)} = I_K$. For model parsimony, we choose $\alpha_0 = 0.5$ in this article so that the weights π_l become sparse.

The distribution for $(\lambda_2^{(s)}, \dots, \lambda_K^{(s)}, \theta^{(s)})$ is independent for each s . The symbol $\text{No}_{(0,2)}$ denotes Gaussian truncated to $(0, 2)$, with upper bound as the maximal possible eigenvalue for normalized Laplacian (Chung and Graham, 1997). The hyper-parameter $w, \sigma_{\lambda,1}^2, \sigma_{\lambda,0}^2, \mu_\theta, \sigma_\theta^2$ are shared among all s .

In (5), we need an equal dimension for all $Q^{(s)}$'s due to limitation of stick-breaking process; hence, we have to use the same K for $s = 1, \dots, S$. However, it does not mean that K is always the ideal dimension for all graphs. To address this, we use a binary $\eta_k^{(s)}$ to put $\lambda_k^{(s)}$'s into two sets: those are close to zero (with $\eta_k^{(s)} = 0$), and those are away from zero and close to $\theta^{(s)}$ (with $\eta_k^{(s)} = 1$). For w , we use weakly informative prior $w \sim \text{Beta}(1, 2)$ to encourage more $\eta_k^{(s)} = 0$. This approximates a model if $K^{(s)}$ were individually chosen,

$$\kappa^{(s)} = 1 + \sum_{k=2}^K \eta_k^{(s)}. \quad (6)$$

as the effective number of small eigenvalues. Since K only acts as the upper bound for $\kappa^{(s)}$, selecting K becomes less important. We assign a Poisson prior to K with μ_K as its prior mean. Figure 2 illustrate the how our distributions accommodate heterogeneity.

2.3 Eigenvalues and Normalized Graph Cut

We now use spectral graph theory to interpret the close-to-zero eigenvalues. As we did not impose order constraint in $\lambda_1^{(s)}, \dots, \lambda_K^{(s)}$, we use the subscript $\cdot_{(k)}$ as the re-ordered index such that $0 < \lambda_{(2)}^{(s)} \leq \dots \leq \lambda_{(K)}^{(s)}$. For ease of notation, we will omit $\cdot^{(s)}$ in this section.

Starting from a simplified scenario, suppose we want to bi-partition (or, ‘cut’) a graph $G = (V, E)$ into two sub-graphs $G_1 = (V_1, E(V_1, V_1))$ and $G_2 = (\bar{V}_1, E(\bar{V}_1, \bar{V}_1))$, with $\bar{V}_1 = V \setminus V_1$ and $E(V_1, V_2)$ the edges between two sets of nodes. Then an intuitive cut corresponds to minimizing the edge weights between G_1 and G_2 ; on the other hand, we want to prevent trivial cuts, such as the one with G_1 as only the most connected node and G_2 as the rest $(n - 1)$ nodes. This leads to ‘normalized min-cut’ (Wu and Schölkopf, 2006)

$$h(G) = \min_{V_1 \subset V, |V_1| \leq \lfloor n/2 \rfloor} \frac{\sum_{i \in V_1, j \in V_2} A_{i,j}}{\sum_{i \in V_1} d_i},$$

where the denominator is total degree in one subgraph. If A is a binary matrix, then $h(G)$ is also known as the Cheeger or isoperimetric constant (Mohar, 1989), representing the bottleneck of the flow through the edges. Friedland and Nabben (2002) proves the Cheeger’s inequality generalized for weighted graph, which relates the cut loss to the eigenvalue:

$$h(G) \leq \sqrt{2\lambda_{(2)}}.$$

To obtain more sub-graphs, we can bi-partition one of the sub-graphs; repeating this κ times, we obtain a total of κ sub-graphs. Louis et al. (2011) show a specific algorithm and prove its smallest cut loss is upper bounded by $(8 \log \kappa) \sqrt{\lambda_{(\kappa)}}$.

Therefore, when $\lambda_{(\kappa)} \approx 0$, there is a clear way to obtain κ sub-graphs with an only small loss in edge weights. Each sub-graph can be viewed as a community.

2.4 Eigenvectors and Sign-based Partitioning

Similarly, for each graph, we reorder the $q_k^{(s)}$ by the associated $\lambda_k^{(s)}$, and use index $_{(k)}$. For ease of notation, we will omit $^{(s)}$ in this section. Examining the off-diagonal part of each adjacency (2) at its expectation

$$\mathbb{E}A_{i,j} = d_i d_j \sum_{k=1}^K (\theta - \lambda_{(k)}) q_{(k)}(i) q_{(k)}(j), \quad i \neq j, \quad (7)$$

where $q_{(k)}(i)$ denotes the i th element in $q_{(k)}$. Note that $d_i > 0, d_j > 0$, and for the first few close-to-zero eigenvalues $k \leq \kappa$, we can assume $\lambda_{(k)} < \theta$. As a result, at each k , an equal sign $q_k(i)q_k(j) > 0$ contributes positively to the $\mathbb{E}A_{i,j}$; while $q_k(i)q_k(j) < 0$ contributes negatively. Therefore, if we are to cut a sub-graph (with node set V^*) using $\{q_{(k)}(i)\}_{i \in V^*}$, the local optimum is simply bi-partitioning V^* into two sets according to the signs of $q_{(k)}(i)$'s. In the simplest case $k = 2$, this is exactly the Fiedler vector partitioning (Fiedler, 1989).

As we fix $q_1 = q_{(1)} = (1/\sqrt{n}, \dots, 1/\sqrt{n})$, due to orthonormality $q_{(k)}^T q_{(k)} = 1$ and $q_1^T q_{(k)} = 0$, we have

$$\sum_{i=1}^n q_{(k)}^2(i) = 1 \quad \sum_{i=1}^n (\sqrt{n})^{-1} q_{(k)}(i) = 0,$$

where the first ensures $q_{(k)}(i)$ cannot be all zero, then second guarantees there must be both pluses and minuses in $q_{(k)}(1), \dots, q_{(k)}(n)$.

Using $q_{(2)} \dots q_{(\kappa)}$, we use the following simple algorithm to obtain κ partitions. Denote the partitions of nodes $V_1^{[k]}, \dots, V_k^{[k]}$ at level k , at the next level $k + 1$:

- For $l = 1, \dots, k$, compute the loss if bi-partitioning $V_l^{[k]}$

$$loss_l^{[k]} = \sum_{i,j \in V_l^{[k]}} [q_{(k+1)}(i)q_{(k+1)}(j)] 1[q_{(k+1)}(i)q_{(k+1)}(j) < 0].$$

- Choose $V_{l^*}^{[k]}$ with $l^* = \arg \min_{l \in \{1, \dots, k\}} \text{loss}_l^{[k-1]}$ and bi-partition: $V_{l^*}^{[k]} = \{i \in V_{l^*}^{[k-1]} : q_k(i) \geq 0\}$, $V_k^{[k]} = \{i \in V_{l^*}^{[k-1]} : q_k(i) < 0\}$. Set other $V_l^{[k+1]} = V_l^{[k]}$, if $l \neq l^*$.

We repeat and stop when $k = \kappa$. To record the community label, we set $c(i) = l$ if $i \in V_l^{[\kappa]}$.

Figure 3 demonstrates how this algorithm works on the data shown in Figure 1.

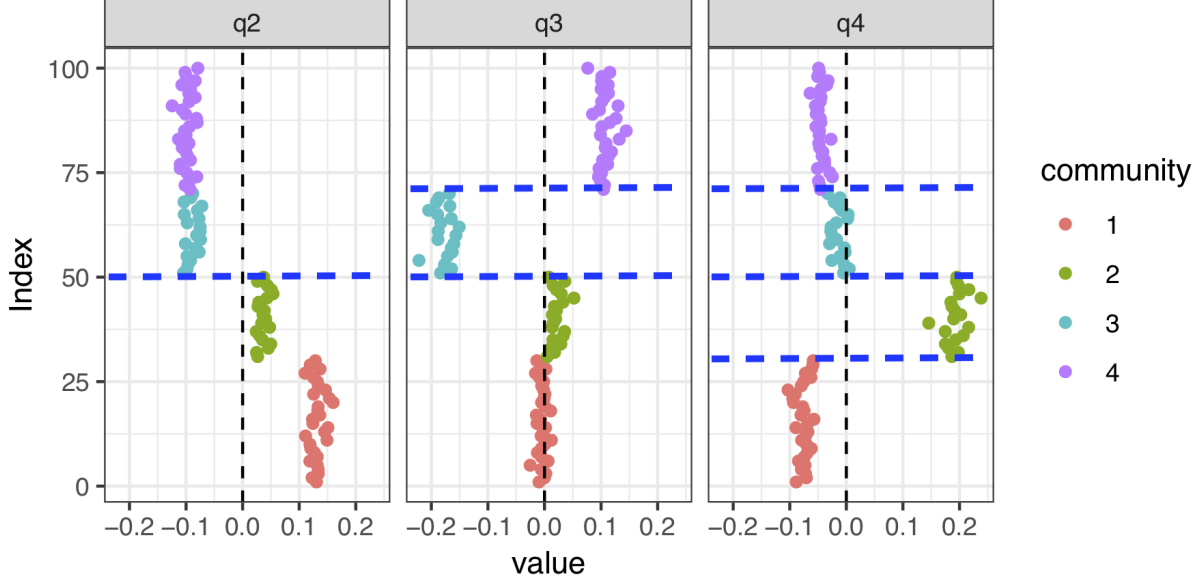


Figure 3: Recursive bi-partitioning using the signs of eigenvectors in $(q_{(2)}, q_{(3)}, q_{(4)})$. At each level, we choose to bi-partition a node set with the largest difference between the opposite-sign elements. The vertical line is the zero line separating different signs; blue horizontal line represents the locally optimal bi-partitioning.

Remark 1. We choose to add only one partition for each $q_{(k)}$, as it is the procedure coherent with the eigenvalue inequality in Section 2.3.

Remark 2. Our algorithm can run almost instantaneously, since it takes one iteration from 2 to κ . This is much faster than other clustering algorithms on eigenvectors, such as

the K -means, which would require multiple iterations and diagnostics for convergence. This computational efficiency is useful for quickly transforming the posterior sample of Q, Λ into c_1, \dots, c_n .

3 Theory

In this section, we provide a theoretic examination of our method. We first show that choosing the number of communities $\kappa^{(s)}$ for the s th graph involves a trade-off between the model resolution and estimation accuracy.

For easy notation, we omit $\cdot^{(s)}$ for now. Assume L is a noisy version of an underlying oracle L_0 (not necessarily having a spiked structure), with L_0 's eigen-matrix denoted by Q_0 . Using the Spiked Laplacian model to produce an estimate $\hat{L} = \hat{Q}(\lambda - I_k\theta)\hat{Q}^T + I_n\theta$, we can quantify the distance between the sub-matrices of \hat{Q} and Q_0 .

Theorem 1 (Trade-off between resolution and estimating accuracy). *Assume the eigenvectors/values in the Spiked Laplacian estimate are ordered such that $\lambda_{(2)} \leq \lambda_{(3)} \dots \leq \lambda_{(K)} < \lambda_{(K+1)} = \dots = \lambda_{(n)} = \theta$, and each element $\hat{L} - L_0$ is sub-Gaussian with the bound parameter σ_e . Denote the sub-matrices formed by the first k columns by $\hat{Q}_{1:k}$ and $Q_{0,1:k}$, then for any $k \in [2, K - 1]$, there exists an orthonormal matrix O*

$$\Pr\left(\|\hat{Q}_{1:k}O - Q_{0,1:k}\|_F \leq \frac{\sqrt{kn}2^{3/2}\sigma_e}{\lambda_{(k+1)} - \lambda_{(k)}}t\right) \geq 1 - \delta_t,$$

where $\delta_t = \exp[-\{t^2/64 - \log(5\sqrt{2})\}n]$.

Remark 3. *The theorem shows that three factors can influence the accuracy: (1) σ_e as the goodness-of-fit of the Spiked Laplacian model; (2) $\lambda_{(k+1)} - \lambda_{(k)}$ as the spectral gap between*

two neighboring eigenvalues; (3) the choice of level k for downstream analysis, such as estimating communities based on $\hat{Q}_{1:k}$. In this article, assuming κ is not too large, our choice of $k = \kappa$ corresponds to the index maximizing the spectral gap, as $\lambda_k \approx 0$ and $\lambda_{k+1} \approx \theta$.

As we assign Gaussian distribution on the eigenvalues, it enjoys posterior conjugacy hence we can integrate out all the eigenvalues. This leads to a marginal form of the eigenvectors

Theorem 2. *The posterior distribution of $Q^{(s)}$'s has the marginal form*

$$\begin{aligned} \Pi(Q^{(1)}, \dots, Q^{(S)} \mid \cdot) &= \prod_{s=1}^S f(Q^{(s)}; L^{(s)}, \eta_1^{(s)}, \dots, \eta_K^{(s)}) \sum_{l=1}^{\infty} \pi_l \delta_{U^{(l)}}(Q^{(s)}), \\ f(Q; L, \eta_1, \dots, \eta_K) &\propto \exp \left\{ \frac{1}{2} \left(\frac{n-K}{2\sigma_e^2} + \frac{1}{\sigma_\theta^2} \right)^{-1} \left[\frac{1}{2\sigma_e^2} \text{tr}([L(I_n - QQ^T)]) + \frac{\mu_\theta}{\sigma_\theta^2} \right]^2 \right. \\ &\quad \left. + \frac{1}{2} \left(\frac{1}{2\sigma_e^2} + \frac{1}{\sigma_{\lambda, \eta_k}^2} \right)^{-1} \sum_{k=1}^K \left[\frac{q_k^T L q_k}{2\sigma_e^2} + \frac{\eta_k \mu_\theta}{\sigma_{\lambda, \eta_k}^2} \right]^2 \right\}. \end{aligned}$$

To understand its effects, we change $I_n - QQ^T = \sum_{k=K+1}^n q_k q_k^T$, and simplifying the negative log- f by ignoring the hyper-parameters, leading to an approximate loss function

$$\sum_{k=1}^K (q_k^T L q_k)^2 + \frac{1}{n-K} \left(\sum_{k=K+1}^n q_k^T L q_k \right)^2.$$

Using $\sum x_i^2 \leq (\sum x_i)^2 \leq 2 \sum x_i^2$ for $x_i \geq 0$, and that L is positive semi-definite (the smallest $\lambda_1 = 0$), we see that each of $(q_k^T L q_k)^2$ with $k > K$ only has $1/(n-K) \sim 2/(n-K)$ times of the weight, compared to those with $k \leq K$. Therefore, the loss function weighs much more heavily on first K eigenvectors than the later ones, which is coherent with our focus on estimating the community structure.

Lastly, we establish the posterior consistency on the estimation of the eigenvectors, under the non-parametric prior distribution. There has been theoretic work on community detection and eigenvector estimation in the graph; however, most have focused on a single graph when the number of nodes n goes to infinity. A fundamental difference here is that we have fixed and bounded n in each graph, but the number of graphs S can grow; hence, a new theory is needed.

In order to avoid a potential dimension discrepancy, we consider an equivalent likelihood based on the *full* eigen-decomposition on the raw observed $L^{(s)} = W^{(s)}\Omega^{(s)}W^{(s)\text{T}}$, where $W^{(s)}$ is an orthonormal matrix and $\Omega^{(s)}$ diagonal. Therefore, $W^{(s)}$ is in a Stiefel manifold $\mathcal{V}^* \subseteq \mathcal{V}^{n,n}$. Similarly, based on parameter Q , we augment the remaining $(n - K)$ eigenvectors, forming an $n \times n$ orthonormal matrix Q^* ; and we let Λ^* be formed by Λ followed by $(n - K)$ repeats of θ on the diagonal.

Each observed $L^{(s)}$ can be considered as generated from

$$f(W^{(s)}, \Omega^{(s)}) = \int f(W^{(s)}, \Omega^{(s)} \mid Q^*, \Lambda^*) P_0(dQ^*) P_0(d\Lambda^*),$$

where $P_0(\cdot)$ denote the prior measure, and the likelihood can be factorized into

$$\begin{aligned} f(W^{(s)}, \Omega^{(s)} \mid Q^*, \Lambda^*) &\propto \exp \left\{ -\frac{1}{4\sigma_e^2} \|W^{(s)}\Omega^{(s)}W^{(s)\text{T}} - Q^*\Lambda^*Q^{*\text{T}}\|_F \right\} \\ &= \underbrace{\text{etr} \left\{ \frac{1}{2\sigma_e^2} Q^*\Lambda^*Q^{*\text{T}}W^{(s)}\Omega^{(s)}W^{(s)\text{T}} \right\}}_{f(W^{(s)} \mid \Omega^{(s)}, Q^*, \Lambda^*)} \underbrace{\text{etr} \left\{ -\frac{1}{4\sigma_e^2} [\Omega^{(s)}\Omega^{(s)} + \Lambda^*\Lambda^*] \right\}}_{f(\Omega^{(s)} \mid \Lambda^*)}. \end{aligned}$$

The former is the density for $W^{(s)} \mid \Omega^{(s)}, Q^*, \Lambda^* \sim \text{Matrix-Bingham}[\Omega^{(s)}, (2\sigma_e^2)^{-1}Q^*\Lambda^*Q^{*\text{T}}]$, where Q^* can be viewed as the location parameter. Therefore, our task is equivalent to showing consistency of $Q^* \in \mathcal{V}^*$, based on a non-parametric mixture prior for Q^* . Using

marginal $f(W^{(s)}) = \int f(W^{(s)}, \Omega) d\Omega$, we can consider a neighborhood of the true density f_0 on the manifold \mathcal{V}^* as

$$B_\epsilon(f_0) = \left\{ f : \left| \int g f \mu(dW) - \int g f_0 \mu(dW) \right| \leq \epsilon, \quad \forall g \in C_b(\mathcal{V}^*) \right\},$$

with C_b the class of continuous and bounded functions, and $\mu(\cdot)$ the Haar measure on \mathcal{V}^* . We show that the probability for the posterior density falling into $B_\epsilon(f_0)$ goes to 1 as $S \rightarrow \infty$.

Theorem 3 (Posterior consistency of the eigenvectors). *Let $W^{(1)}, \dots, W^{(S)}$ be the eigenvectors drawn i.i.d from some true density f_0 . then for all $\epsilon > 0$, as $S \rightarrow \infty$,*

$$\Pi(B_\epsilon(f_0) \mid W^{(1)}, \dots, W^{(S)}) = \frac{\int_{B_\epsilon(f_0)} \prod_{s=1}^S f(W^{(s)}) \Pi(df)}{\int \prod_{s=1}^S f(W^{(s)}) \Pi(df)} \rightarrow 1 \text{ a.s. } Pf_0^\infty,$$

with Pf_0^∞ the true probability measure for $(W^{(1)}, W^{(2)}, \dots)$.

4 Posterior Computation and Inference

When estimating the mixture model for $Q^{(s)}$, we use a latent assignment $z_s \in \{1, 2, \dots\}$ for each graph, such that $Q^{(s)} = U^{(l)}$ if $z_s = l$. Then log-likelihood-prior given $\{z_s\}$ becomes

$$\begin{aligned} & \sum_{l=1}^g \sum_{s: z_s=l} -\frac{1}{4\sigma_e^2} \|L^{(s)} - \theta I_n - U^{(l)}(\Lambda^{(s)} - \theta^{(s)} I_K) U^{(l)\top}\|_F^2 \\ &= -\sum_{s=1}^S \frac{1}{4\sigma_e^2} \left\{ \text{tr}[(\Lambda^{(s)} - \theta^{(s)} I_K)^2] + \|L - \theta^{(s)} I_n\|_F^2 \right\} \\ &+ \sum_{l=1}^g \sum_{s: z_s=l} \frac{1}{2\sigma_e^2} \text{tr}[(\theta^{(s)} I_n - L^{(s)}) U^{(l)} (\theta^{(s)} I_K - \Lambda^{(s)}) U^{(l)\top}]. \end{aligned}$$

For simplicity, we denote $F_s = \alpha_1 I_n - L^{(s)}$ and $G_s = \theta^{(s)} I_K - \Lambda^{(s)}$, where α_1 is a constant such that all F_s 's are positive definite (we choose a $\alpha_1 > 2$ in the article as the eigenvalues of normalized Laplacian are always less or equal to 2); hence, the log-posterior for $U^{(l)}$ is proportional to the product of matrix Bingham- $\{F_s/(2\sigma_e^2), G_s\}$,

$$\Pi(U^{(l)} | \cdot) \propto \exp \left\{ \frac{1}{2\sigma_e^2} \sum_{s:z_s=l} \text{tr}(F_s U^{(l)} G_s U^{(l)\text{T}}) \right\} \text{etr}(\Omega M^{\text{T}} U^{(l)}), \quad (8)$$

which lacks closed form for sampling. To solve this problem, we propose a new data augmentation for matrix Bingham distribution.

4.1 Data Augmentation for Matrix Bingham Distribution

To bypass the challenge of (8) in the quadratic term of $U^{(l)}$, we extend the Gaussian integral trick (Zhang et al., 2012) on Stiefel manifold. Consider a random matrix $R_s \in \mathbb{R}^{K \times n}$

$$\Pi(R_s | U^{(l)}) \propto |F_s|^{-K/2} |G_s|^{-n/2} \text{etr} \left\{ -\frac{1}{2\sigma_e^2} F_s^{-1} (R_s - G_s U^{(l)\text{T}} F_s)^{\text{T}} G_s^{-1} (R_s - G_s U^{(l)\text{T}} F_s) \right\}, \quad (9)$$

which is a matrix Gaussian random variable $\text{Mat-No}(G_s U^{\text{T}} F_s, G_s \sigma_e^2, F_s)$. Given R_s , all quadratic terms are canceled, leading to the conditional density

$$\Pi(U^{(l)} | \{R_s\}_{s:z_s=l}) \propto \text{etr} \left(\frac{1}{\sigma_e^2} \sum_{s:z_s=l} R_s U^{(l)} + \Omega M^{\text{T}} U^{(l)} \right), \quad (10)$$

which is now a matrix Langevin distribution $\text{vMF}(\sum_{s:z_s=l} R_s / \sigma_e^2 + \Omega M^{\text{T}})$.

4.2 Gibbs Sampling

We use Gibbs sampling to obtain the posterior sample. To accelerate the update of z_s , we use the marginal form from Theorem 2. For the global noise variance σ_e^2 , we assume

improper prior $\pi_0(\sigma_e^2) = \sigma_e^{-2}$; to simplify the computation, we approximate the Dirichlet process mixture model with a truncated version, setting the number of mixture components to g and using $\text{Dir}(\alpha_0/g, \dots, \alpha_0/g)$ (in this paper, we use $g = 30$ and $\alpha_0 = 0.5$).

The posterior sampling proceeds in the following steps:

1. Sample R_s from (9).
2. Sample $U^{(l)}$ from (10).
3. Sample from the categorical distribution

$$z_s \sim \Pi(z_s \mid \cdot) \propto \pi_l 1(z_s = l) \exp \left\{ \frac{1}{2} \left(\frac{n-K}{2\sigma_e^2} + \frac{1}{\sigma_\theta^2} \right)^{-1} \left[\frac{1}{2\sigma_e^2} \text{tr}([L^{(s)}(I_n - U^{(l)}U^{(l)T})]) + \frac{\mu_\theta}{\sigma_\theta^2} \right]^2 \right. \\ \left. + \frac{1}{2} \left(\frac{1}{\sigma_{\lambda, \eta_k^{(s)}}^2} + \frac{1}{2\sigma_e^2} \right)^{-1} \sum_{k=1}^K \left[\frac{u_k^{(l)T} L^{(s)} u_k^{(l)}}{2\sigma_e^2} + \frac{\eta_k^{(s)} \mu_\theta}{\sigma_{\lambda, \eta_k^{(s)}}^2} \right]^2 \right\},$$

with $1(\cdot)$ the indicator function, update $Q^{(s)} = U^{(z_s)}$.

4. Sample $(\pi_1, \pi_2, \dots, \pi_g) \sim \text{Dir}(\alpha_0/g + \sum 1(z_s = 1), \alpha_0/g + \sum 1(z_s = 2), \dots, \alpha_0/g + \sum 1(z_s = g))$.
5. Sample for $k = 2, \dots, K$

$$\lambda_k^{(s)} \sim \text{No}_{(0,2)} \left\{ \left(\frac{1}{\sigma_{\lambda, \eta_k^{(s)}}^2} + \frac{1}{2\sigma_e^2} \right)^{-1} \left[\frac{q_k^{(s)T} L^{(s)} q_k^{(s)}}{2\sigma_e^2} + \frac{\eta_k^{(s)} \mu_\theta}{\sigma_{\lambda, \eta_k^{(s)}}^2} \right], \left(\frac{1}{\sigma_{\lambda, \eta_k^{(s)}}^2} + \frac{1}{2\sigma_e^2} \right)^{-1} \right\}.$$

6. Sample from the Bernoulli for $k = 2, \dots, K$

$$\eta_k^{(s)} \sim \Pi(\eta_k^{(s)} \mid \cdot) \propto \\ 1(\eta_k^{(s)} = 0)(1-w) \text{No}_{(0,2)} \left\{ \left(\frac{1}{\sigma_{\lambda,0}^2} + \frac{1}{2\sigma_e^2} \right)^{-1} \left[\frac{q_k^{(s)T} L^{(s)} q_k^{(s)}}{2\sigma_e^2} \right], \left(\frac{1}{\sigma_{\lambda,0}^2} + \frac{1}{2\sigma_e^2} \right)^{-1} \right\} \\ + 1(\eta_k^{(s)} = 1)w \text{No}_{(0,2)} \left\{ \left(\frac{1}{\sigma_{\lambda,1}^2} + \frac{1}{2\sigma_e^2} \right)^{-1} \left[\frac{q_k^{(s)T} L^{(s)} q_k^{(s)}}{2\sigma_e^2} + \frac{\mu_\theta}{\sigma_{\lambda,1}^2} \right], \left(\frac{1}{\sigma_{\lambda,1}^2} + \frac{1}{2\sigma_e^2} \right)^{-1} \right\}.$$

7. Sample

$$\theta^{(s)} \sim \text{No}_{(0,2)} \left\{ \left(\frac{n-K}{2\sigma_e^2} + \frac{1}{\sigma_\theta^2} \right)^{-1} \left[\frac{1}{2\sigma_e^2} \left(\sum_i L^{(s)}(i, i) - \sum_k q_k^{(s)\text{T}} L^{(s)} q_k^{(s)} \right) + \frac{\mu_\theta}{\sigma_\theta^2} \right], \right. \\ \left. \left(\frac{n-K}{2\sigma_e^2} + \frac{1}{\sigma_\theta^2} \right)^{-1} \right\}.$$

8. Sample for $i = 1, \dots, n$

$$L_{i,i}^{(s)} \sim \text{No} \left\{ \left[Q^{(s)} (\Lambda^{(s)} - \theta^{(s)} I_K) Q^{(s)\text{T}} \right]_{(i,i)} + \theta^{(s)}, 2\sigma_e^2 \right\}.$$

9. Sample

$$\sigma_e^2 \sim \text{Inv-Gamma} \left\{ \frac{n^2 S}{2}, \frac{1}{4} \sum_{s=1}^S \|L^{(s)} - \theta I_n - Q_*^{(l)} (\Lambda^{(s)} - \theta^{(s)} I_K) Q_*^{(l)\text{T}}\|_F^2 \right\}.$$

For the hyper-parameter $\mu_\theta, \sigma_\theta^2, \sigma_{\lambda,0}^2$ and $\sigma_{\lambda,1}^2$, they lack closed-form conditionals; however, since their uncertainty is less important, we use empirical Bayes prior by setting them as the sample mean and variance in θ and λ after running the algorithm for a few hundred iterations.

In all experiments, we use $\mu_K = 10$ as the prior mean for K . As sampling over discrete K is inefficient, we run several chains over a range of K and compute the marginal posterior density. For easy analysis, we use the K corresponding to the maximum marginal posterior; model averaging over different K is another possibility, although it adds up complication when analyzing the discrete community partition.

Via the sign-based algorithm, we obtain the community labels $c_i^{(s)}$ based on each posterior sample of $Q^{(s)}$ and $\kappa^{(s)}$. To quantify their uncertainty, we then marginalize over the posterior samples of $Q^{(s)}, \kappa^{(s)}$. To bypass the label-switching issue in $c^{(s)}(i)$, we focus on pairwise comparison and compute the equal-label probability $\text{pr}\{c_i^{(s)} = c_j^{(s)}\}$.

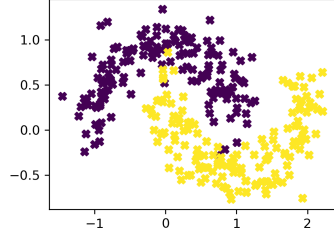
5 Simulation Study

5.1 Uncertainty Quantification using Graph Laplacian

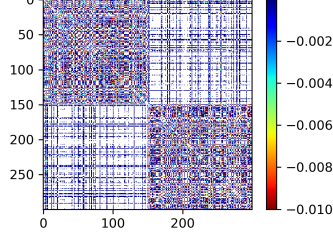
We first assess the uncertainty quantification performance in the small graph community detection. We now use a single graph setting for the clear exposition.

To obtain a weighted graph with overlapping communities, we first sample the latent positions y_i 's near two moon manifolds [Figure 4(a)], then compute the pairwise similarity between latent position $[A_{i,j} = \exp(-10\|y_i - y_j\|_2)]$ as the edge weight. The major uncertainty resides in the part where two manifolds are close.

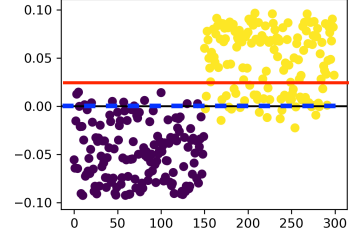
Figure 4(b)(c) plot the normalized Laplacian L and the second eigenvector \hat{q}_2 of L , based on $n = 300$. Clearly, the zero line used by the sign-based partition is a good division between two communities; whereas applying K-means on this eigenvector, as typically used in the stochastic block model, can give a sub-optimal cut due to the overlap.



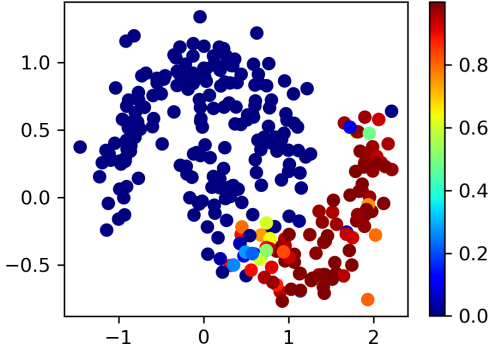
(a) Oracle latent positions $y_i \in \mathbb{R}^2$ used to generate a weighted graph, colored by the true community labels.



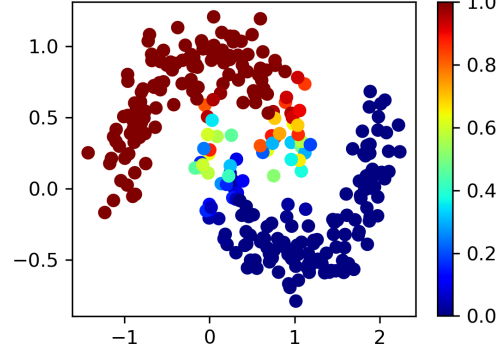
(b) Normalized Laplacian L based on the weighted graph $A_{i,j} = \exp(-10\|y_i - y_j\|_2)$.



(c) Elements of the second eigenvector $\hat{q}_2(i)$ of L . Decision boundary: red— K-means; blue — sign-based.



(d) Uncertainty $\text{pr}(c_i = 1)$ estimated using Gaussian mixture on a single estimate of $\hat{q}_2(i)$.



(e) Uncertainty $\text{pr}(c_i = 1)$ estimated using our sign-based algorithm on each posterior sample point of $q_2(i)$.

Figure 4: Simulated experiment of partitioning nodes into two communities, with true latent positions originated near two manifolds (a). Due to the proximity, there is substantial uncertainty. (c) shows that sign-based partitioning on the eigenvector is more accurate compared to typical clustering algorithm; (d) shows that using one frame of eigenvector together with Gaussian mixture model underestimates the uncertainty; whereas (e) shows that using the posterior sample of eigenvector gives more accurate estimate.

n	100	300	500
Sign-based on \hat{q}_2	(0.14 ± 0.11)	(0.09 ± 0.04)	(0.08 ± 0.04)
K-means on \hat{q}_2 (SBM)	(0.31 ± 0.15)	(0.15 ± 0.08)	(0.10 ± 0.06)
Bayesian SBM	(0.30 ± 0.14)	(0.14 ± 0.07)	(0.12 ± 0.07)
Gaussian mixture on \hat{q}_2	(0.32 ± 0.20)	(0.21 ± 0.09)	(0.10 ± 0.06)

Table 1: Misclassification error using different algorithms to partition the nodes. Sign-based partition on the eigenvector has a clear advantage especially when n is small. The numbers are the mean error \pm its standard deviation, based on 50 repeats of experiments in each setting.

In addition, we compare our method against the alternative idea of ‘random partition on a fixed Q ’ — first extracting the eigenvectors of the raw Laplacian, then using on a Gaussian mixture model to quantify the uncertainty. As shown in Figure 4(d), fixing the eigenvectors at the end of the first stage can severely under-estimate the variability, with most of the probabilities too close to zero/one. On the other hand, as shown by the panel (e), the deterministic transform on each posterior sample of Q gives more accurate estimates on the probabilities.

We compare our method against popular alternatives, with different number of nodes $n \in \{100, 300, 500\}$. The results are listed in Table 1.

5.2 Fitting Multiple Graphs

We experiment with multiple graphs with heterogeneity. We first generate a set of five possible community structures, each represented by a binary matrix (denoted by $W^{(l)}$) of size 300×6 ; each row has one 1 and five 0's, encoding the ground truth of the community labels in $1, \dots, 6$. To generate a graph, we randomly draw one of five patterns as $\tilde{W}^{(s)}$ and a non-negative random vector $\tilde{\Lambda}$, producing the adjacency matrix via $A^{(s)} = \tilde{W}^{(s)}\tilde{\Lambda}\tilde{W}^{(s)\text{T}} + \tilde{\mathcal{E}}^{(s)}$, with $\tilde{\mathcal{E}}^{(s)}$ a Gaussian noise matrix and $\tilde{e}_{i,j}^{(s)} = \tilde{e}_{j,i}^{(s)} \sim \text{No}(0, 1)$.

We compare our model against several popular alternatives: (1) simple averaging of all graphs followed by the use of stochastic block model, (2) co-regularized stochastic block model/ spectral clustering (Kumar et al., 2011), (3) clustering the graphs into five groups, and applying the stochastic block model in each group, (4) independent stochastic block model for each graph. The first two competitors produce only one partitioning, while the latter two accommodate the heterogeneity.

We compute two benchmark scores: normalized mutual information (NMI), as the similarity between the estimated community labels to the ground truth in each graph; the RMSE between the individual $L^{(s)}$ and the smoothed $\hat{L}^{(s)}$, as the goodness of fit measurement.

As shown in Table 2, our proposed model has the highest accuracy in estimating the community labels, followed by the two-stage estimator that clusters the graphs first then partitions the nodes via the stochastic block model. The performance of individual stochastic block models is much worse, likely due to it does not borrow information among graphs, and the node number is not too large. In the goodness-of-fit, the individual stochastic block models

have the best score as it has the highest flexibility; our model has a slightly larger error; however, it is much lower than the other competitors.

Benchmark Scores	NMI (higher is better)	RMSE ($\times 10^{-3}$, lower is better)
Spiked Laplacian Graphs	0.85 ± 0.04	1.9 ± 0.2
Average+SBM	0.21 ± 0.15	9.2 ± 2.5
Co-regularized SBM	0.25 ± 0.11	10.2 ± 4.5
Clustering Graphs + SBMs	0.67 ± 0.24	5.5 ± 1.5
Individual SBMs	0.45 ± 0.13	1.2 ± 0.2

Table 2: Benchmark of the fitting models to a population of heterogeneous graphs . When computing the RMSE, for the Spiked Laplacian Graphs, we obtain $\hat{L}^{(s)}$ from the spiked representation taking individual $\kappa^{(s)}$ as the truncated dimension, averaging over the posterior sample; for the other four, we define $\hat{L}^{(s)}$ as the truncated spectral representation $\hat{Q}\hat{\Lambda}\hat{Q}$ with $(\hat{Q}, \hat{\Lambda})$ corresponding to the top 6 dimensions (as the ground truth dimension for data generation).

6 Data Application: Characterizing Heterogeneity in Human Working Memory Study

We now use the proposed model for a neuroscience study of working memory. The data are collected from a study of human brain functional connectivities (Hu et al., 2019). Each subject was asked to do the Sternberg verbal working memory task, which involved memorizing a list of six numbers, followed by a memory retrieval task that requires the

subject to answer if a number was among the six shown earlier. The EEG signals were captured from 128 electrode channels placed over each subject’s head, and then a 128×128 connectivity network is estimated during the retrieval period. Each network contains weights between 0 and 1, and there are $S = 1,329$ networks.

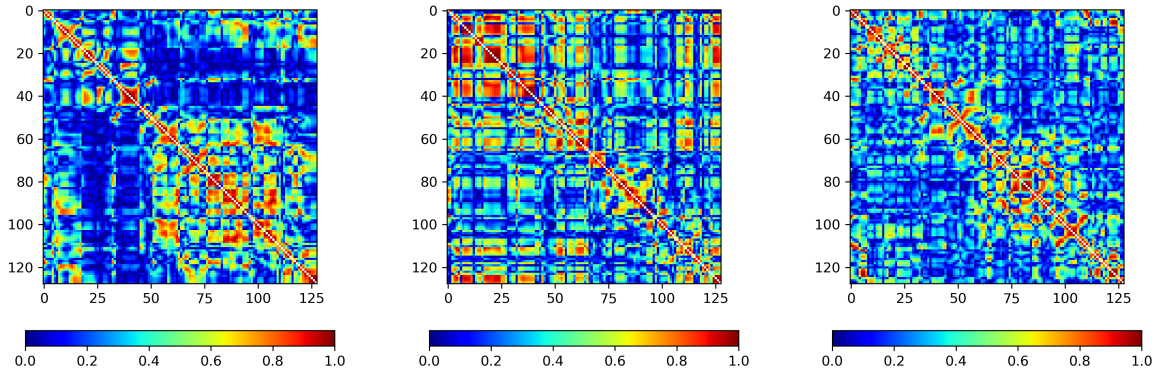


Figure 5: Raw adjacency graphs showing the brain functional connectivities for three individuals performing memory retrieval task. Even with the noise present, we can see the heterogeneity among those subjects.

Those subjects show great heterogeneity during the memory retrieval task. For example, as shown by three selected adjacency matrices $A^{(s)}$ in Figure 5, those memory-related connectivities can have a different concentration in the front or back of the head (panel a or b, with spatial coordinates, plotted in Figure a), or, they are more localized in smaller regions (panel c).

We apply our proposed model on this dataset, and run MCMC for 30,000 steps, and use the last 20,000 steps for inference. In the result, most of the posterior samples contain six distinct $U^{(l)}$ ’s as the clustered eigenmatrix values; among those we present the three

corresponding to the raw $A^{(s)}$ shown above, in terms of the fitted Laplacian matrices. The other three seem to correspond to smaller variations, so we leave them in the supplementary file. The proportions for these six groups are 25.6%, 24.1%, 16.1%, 14.7%, 15.2% and 4.3%, as estimated in the posterior mean of allocation z_s .

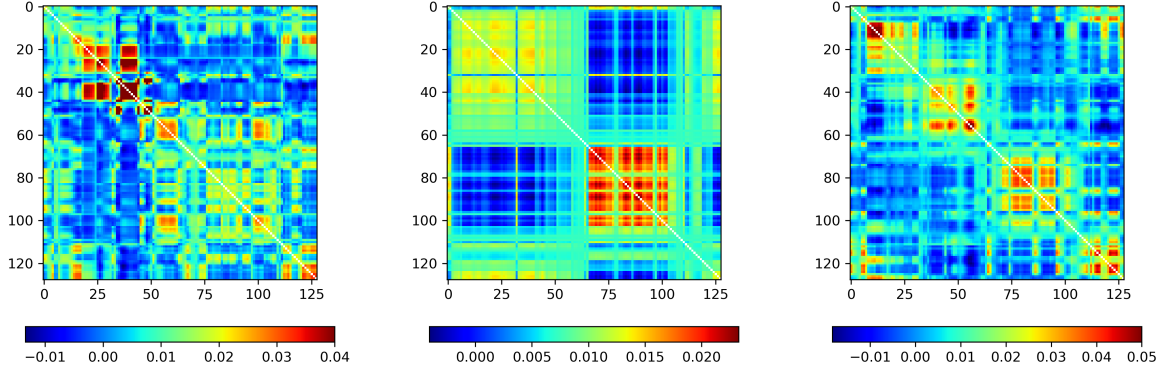
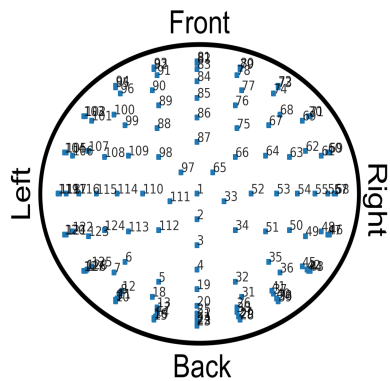
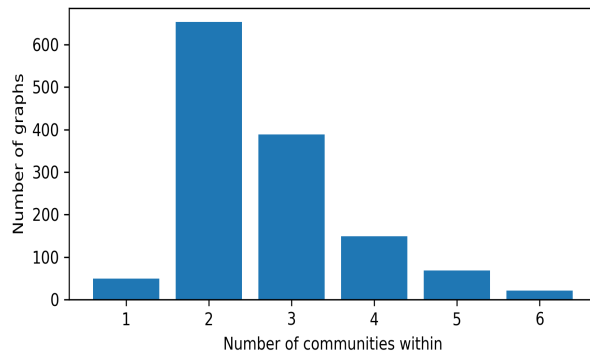


Figure 6: Fitted Laplacian shows the structure underneath each raw connectivity matrix.

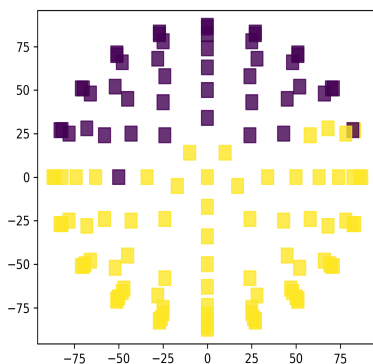
We then evaluate the community structures in each graph. As shown in Figure 7(a), the model discovers $1 \sim 6$ communities from these graphs, as estimated by $\kappa^{(s)}$ from (6). To understand its scientific meaning, we plot the community labels mapped to the spatial coordinates. Panel (c) and (d) show that most of the graphs have only two clear communities, although the division can be quite different in the dominating area either in the front or in the back. Panel (e) shows a very distinct pattern with four communities, partitioned as the outer-front, mid-front, left-back, right-back.



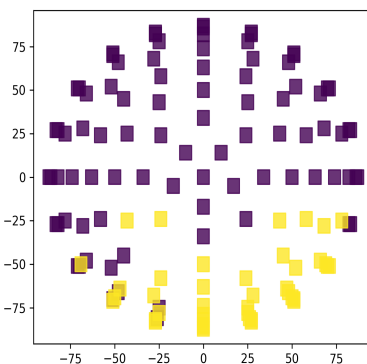
(a) Coordinates of the EEG sensors, viewed from the top of the head.



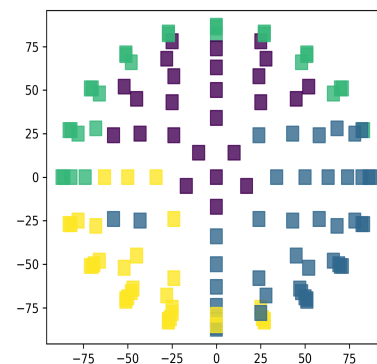
(b) Histogram of the number of communities in all subjects.



(c) The subject has two communities, with larger one near the back.



(d) The subject has two communities, with larger one near the front.



(e) The subject has four communities: outer-front, mid-front, left-back, right-back.

Figure 7: Community structure for each brain scan from multiple subjects in the working memory study.

7 Discussion

In this article, we propose a generative graph model based on the Laplacian, allowing us to exploit the spectral graph theory to conduct flexible community detection in a population of heterogeneous graphs. Our model can be considered as a general idea to introduce Bayesian toolboxes into the spectral graph framework. There are several extensions worth exploring in future work. First, if the goal is to generate a new graph with binary $A_{i,j}$, such as in link prediction, then it could adopt a Bernoulli distribution associated with a canonical link. Second, if those graphs have some known covariance structure, such as repeated measurement or temporal effect, then it could take an alternative distribution on the eigenmatrix or eigenvalues to incorporate those structures. Lastly, when it comes to a large graph, it is interesting to consider θ not as one constant but a step function corresponding to different coarse-grain resolutions of the model.

References

- Airoldi, E. M., D. M. Blei, S. E. Fienberg, and E. P. Xing (2008). Mixed Membership Stochastic Blockmodels. *Journal of Machine Learning Research* 9(Sep), 1981–2014.
- Bhattacharya, A. and D. B. Dunson (2010). Nonparametric Bayesian Density Estimation on Manifolds With Applications to Planar Shapes. *Biometrika* 97(4), 851–865.
- Cai, D., T. Campbell, and T. Broderick (2016). Edge-Exchangeable Graphs and Sparsity. In *Advances in Neural Information Processing Systems*, pp. 4249–4257.
- Caron, F. and E. B. Fox (2017). Sparse Graphs Using Exchangeable Random Measures. *Journal of the Royal Statistical Society: Series B (Statistical Methodology)* 79(5), 1295–1366.
- Chung, F. R. and F. C. Graham (1997). *Spectral Graph Theory*. Number 92. American Mathematical Soc.

- Donoho, D. L., M. Gavish, and I. M. Johnstone (2018). Optimal Shrinkage of Eigenvalues in the Spiked Covariance Model. *Annals of Statistics* 46(4), 1742.
- Durante, D., D. B. Dunson, and J. T. Vogelstein (2017). Nonparametric Bayes Modeling of Populations of Networks. *Journal of the American Statistical Association* 112(520), 1516–1530.
- Fiedler, M. (1989). Laplacian of Graphs and Algebraic Connectivity. *Banach Center Publications* 25(1), 57–70.
- Friedland, S. and R. Nabben (2002). On Cheeger-Type Inequalities for Weighted Graphs. *Journal of Graph Theory* 41(1), 1–17.
- Geng, J., A. Bhattacharya, and D. Pati (2019). Probabilistic Community Detection With Unknown Number of Communities. *Journal of the American Statistical Association* 114(526), 893–905.
- Hoff, P. D. (2009, January). Simulation of the matrix Bingham–von Mises–Fisher Distribution, With Applications to Multivariate and Relational Data. *Journal of Computational and Graphical Statistics* 18(2), 438–456.
- Hoff, P. D., A. E. Raftery, and M. S. Handcock (2002). Latent Space Approaches to Social Network Analysis. *Journal of the American Statistical Association* 97(460), 1090–1098.
- Hu, Z., C. M. Barkley, S. E. Marino, C. Wang, A. Rajan, K. Bo, I. B. H. Samuel, and M. Ding (2019). Working Memory Capacity Is Negatively Associated With Memory Load Modulation of Alpha Oscillations in Retention of Verbal Working Memory. *Journal of Cognitive Neuroscience*, 1–13.
- Karrer, B. and M. E. Newman (2011). Stochastic Blockmodels and Community Structure in Networks. *Physical review E* 83(1), 016107.
- Koev, P. and A. Edelman (2006). The Efficient Evaluation of the Hypergeometric Function of a Matrix Argument. *Mathematics of Computation* 75(254), 833–846.
- Kumar, A., P. Rai, and H. Daume (2011). Co-Regularized Multi-View Spectral Clustering. In *Advances in Neural Information Processing Systems*, pp. 1413–1421.
- Lin, L., V. Rao, and D. Dunson (2017). Bayesian Nonparametric Inference on the Stiefel Manifold. *Statistica Sinica*, 535–553.
- Louis, A., P. Raghavendra, P. Tetali, and S. Vempala (2011). Algorithmic Extensions

- of Cheeger’s Inequality to Higher Eigenvalues and Partitions. In *Approximation, Randomization, and Combinatorial Optimization. Algorithms and Techniques*, pp. 315–326. Springer.
- Mohar, B. (1989). Isoperimetric Numbers of Graphs. *Journal of Combinatorial Theory, Series B* 47(3), 274–291.
- Mukherjee, S. S., P. Sarkar, and L. Lin (2017). On Clustering Network-Valued Data. In *Advances in Neural Information Processing Systems*, pp. 7071–7081.
- Ng, A. Y., M. I. Jordan, and Y. Weiss (2002). On Spectral Clustering: Analysis and an Algorithm. In *Advances in Neural Information Processing Systems*, pp. 849–856.
- Robins, G., P. Pattison, Y. Kalish, and D. Lusher (2007). An Introduction to Exponential Random Graph (p*) Models for Social Networks. *Social Networks* 29(2), 173–191.
- Shen, X., F. Tokoglu, X. Papademetris, and R. T. Constable (2013). Groupwise Whole-Brain Parcellation From Resting-State fMRI Data for Network Node Identification. *Neuroimage* 82, 403–415.
- Tao, T. (2012). *Topics in Random Matrix Theory*, Volume 132. American Mathematical Soc.
- van der Pas, S., A. van der Vaart, et al. (2018). Bayesian Community Detection. *Bayesian Analysis* 13(3), 767–796.
- Wainwright, M. J. (2019). *High-Dimensional Statistics: a Non-Asymptotic Viewpoint*, Volume 48. Cambridge University Press.
- Williamson, S. A. (2016). Nonparametric Network Models for Link Prediction. *Journal of Machine Learning Research* 17(1), 7102–7121.
- Wu, M. and B. Schölkopf (2006). Normalized Cuts and Image Segmentation. In *Advances in Neural Information Processing Systems*, pp. 1529–1536.
- Yu, Y., T. Wang, and R. J. Samworth (2014). A Useful Variant of the Davis–Kahan Theorem for Statisticians. *Biometrika* 102(2), 315–323.
- Zhang, Y., Z. Ghahramani, A. J. Storkey, and C. A. Sutton (2012). Continuous Relaxations for Discrete Hamiltonian Monte Carlo. In *Advances in Neural Information Processing Systems*, pp. 3194–3202.

Appendix

Proof of Theorem 1

Proof. For simplicity, we omit $\cdot^{(s)}$ in the proof and use σ_e for σ_{e0} . The proof consists of four major parts

1. Using Davis-Kahan Theorem

Let $E = \tilde{L} - L$, using Theorem 2 of (Yu et al., 2014) with $r = 2$ and $s = k$, we obtain

$$\begin{aligned} \|Q_0 - QO\|_F &\leq \frac{2^{3/2} \min(K^{1/2} \|E\|_{op}, \|E\|_F)}{\lambda_{k+1} - \lambda_k} \\ &\leq \frac{2^{3/2} (K^{1/2} \|E\|_{op})}{\lambda_{k+1} - \lambda_k} \end{aligned}$$

where $\|E\|_{op}$ is the operator norm such $\|E\|_{op} = \sup_{\|x\|=1} \|Ex\|$.

2. Discretizing $\mathbb{S}^n = \{x : \|x\| = 1\}$ using maximal ϵ -net:

Following Tao (2012), let $N_\epsilon \subset \mathbb{S}^n$ be an ϵ -net with $\epsilon \in (0, 1)$, such that for any two $x \in N_\epsilon, x' \in N_\epsilon, \|x - x'\| \geq \epsilon$. Maximizing over the number of included points in \mathbb{S}^n , we obtain a maximal ϵ -net N_ϵ^0 . Clearly, the balls with centers $x \in N_\epsilon^0$ and radius $\epsilon/2$ are disjoint, and all covered by a large ball centered at the origin with radius $1 + \epsilon/2$, hence

$$|N_\epsilon^0| \leq \left(\frac{\epsilon/2 + 1}{\epsilon/2}\right)^n = \left(\frac{\epsilon + 2}{\epsilon}\right)^n.$$

On the other hand, for any $y \in \mathbb{S}^n$, there is at least one $x \in N_\epsilon^0 : \|x - y\| \leq \epsilon$, otherwise y can be added to the net, contradicting the maximal condition.

Choosing $y \in \mathbb{S}^n$ that attains $\|Ey\| = \|E\|_{op}$, and its associated $x \in N_\epsilon^0 : \|x - y\| \leq \epsilon$

$$\|E\|_{op} - \|Ex\| = \|Ey\| - \|Ex\| \leq \|E(y - x)\| \leq \|E\|_{op} \epsilon,$$

where we used triangle inequality and $f(x) = \|Ex\|$ is $\|E\|_{op}$ -Lipschitz.

Therefore, $\|E\|_{op} \geq t$ implies at least one $x \in N_\epsilon^0 : \|Ex\| \geq (1 - \epsilon)t$.

$$\begin{aligned} \text{pr}(\|E\|_{op} \geq t) &\leq \text{pr}\left(\bigcup_{x \in N_\epsilon^0} \|Ex\| \geq (1 - \epsilon)t\right) \\ &\leq |N_\epsilon^0| \text{pr}\left(\|Ex\| \geq (1 - \epsilon)t, \text{ where } x \in \mathbb{S}^n\right) \end{aligned}$$

where the last inequality is due to union bound.

3. Concentration inequality for $\|Ex\|$

Let B be an $n \times n$ matrix with $b_{i,j}$ independent and sub-Gaussian with σ_e^2 . Then for each element Bx

$$\begin{aligned}\mathbb{E} \exp\{t B_j^T x\} &= \mathbb{E} \exp\{t \sum_{k=1}^n x_k b_{j,k}\} \\ &= \prod_{k=1}^n \mathbb{E} \exp\{t x_k b_{j,k}\} \\ &\leq \prod_{k=1}^n \exp\{t^2 \sigma_e^2 x_k^2 / 2\} \\ &= \exp\{t^2 \sigma_e^2 / 2\}\end{aligned}$$

where the inequality is due to sub-Gaussianity, and last equality due to $\|x\| = 1$. Therefore, each $Z_j = B_j x$ is sub-Gaussian as well. By Wainwright (2019), this is equivalent to

$$\mathbb{E} \exp\left(\frac{\kappa Z_j^2}{2\sigma_e^2}\right) \leq (1 - \kappa)^{-1/2} \quad (11)$$

for all $\kappa \in (0, 1)$.

Since E is symmetric, let $E = E_U + E_L$, with E_U the upper triangular matrix including the diagonal and E_L the lower triangular. We have

$$\|Ex\|^2 = \|E_U x + E_L x\|^2 \leq (\|E_U x\| + \|E_L x\|)^2 \leq 2(\|E_U x\|^2 + \|E_L x\|^2)$$

By Cauchy-Schwarz

$$\begin{aligned}\mathbb{E} \exp\left(\frac{\kappa \|Ex\|^2}{2\sigma_e^2}\right) &\leq \mathbb{E} \exp\left(\frac{2\kappa (\|E_U x\|^2 + \|E_L x\|^2)}{2\sigma_e^2}\right) \\ &\leq \sqrt{\mathbb{E} \exp\left(\frac{4\kappa \|E_U x\|^2}{2\sigma_e^2}\right) \mathbb{E} \exp\left(\frac{4\kappa \|E_L x\|^2}{2\sigma_e^2}\right)}\end{aligned}$$

Since E_U and E_L are results of sub-Gaussian elements and zeros, hence are also sub-Gaussian with σ_e^2 , multiplying (11) over $j = 1, \dots, n$ for each matrix

$$\mathbb{E} \exp\left(\frac{\kappa \|Ex\|^2}{2\sigma_e^2}\right) \leq \sqrt{(1 - 4\kappa)^{-n/2} (1 - 4\kappa)^{-n/2}} = (1 - 4\kappa)^{-n/2}$$

where $\kappa \in (0, 1/4)$. Using Markov inequality

$$\Pr(\|Ex\| \geq t) = \Pr\left(\exp\left(\frac{\kappa \|Ex\|^2}{2\sigma_e^2}\right) \geq \exp\left(\frac{\kappa t^2}{2\sigma_e^2}\right)\right) \leq (1 - 4\kappa)^{-n/2} \exp\left(-\frac{\kappa t^2}{2\sigma_e^2}\right).$$

4. Combining results to yield concentration inequality

Therefore,

$$\text{pr}(\|E\|_{op} \geq t) \leq \left(\frac{\epsilon + 2}{\epsilon}\right)^n (1 - 4\kappa)^{-n/2} \exp\left(-\frac{\kappa(1 - \epsilon)^2 t^2}{2\sigma_e^2}\right)$$

Letting $t = c_1 \sqrt{n} \sigma_e$, $\kappa = 1/8$ and $\epsilon = 1/2$, we have

$$\text{pr}(\|E\|_{op} \geq c_1 \sqrt{n} \sigma_e) \leq \exp[-\{c_1^2/64 - \log(5\sqrt{2})\}n] \equiv \delta$$

Therefore,

$$\|Q - \hat{Q}\hat{O}\|_F \leq \frac{2^{3/2} K^{1/2} c_1 \sqrt{n} \sigma_e}{\theta - \lambda_K}$$

with probability greater than $1 - \delta$.

□

Proof of Theorem 2

Proof. This proof is inspired by early work of Bhattacharya and Dunson (2010) and Lin et al. (2017) related to density estimation on compact manifold.

For simplicity, we omit $\cdot^{(s)}$ for now and let $D = \Lambda^*$ and $B = \Omega$. Without loss of generality, we assume the diagonal of B are ordered $0 = b_1 \leq b_2 \leq \dots \leq b_n$. The parameter Q^* follows a matrix Bingham distribution

$$g(Q^*; \sigma_e^2) \Pi(dQ^*) = Z^{-1}(\sigma_e^2, D, B) \text{etr} \left\{ \frac{1}{2\sigma_e^2} D Q^{*\text{T}} W B W^{\text{T}} Q^* \right\} \Pi(dQ^*)$$

where Z is a normalizing constant.

Our goal is to show there exists an neighborhood D_ϵ for σ_e^2 , such that

$$\Delta = \sup_{W \in \mathcal{V}^*, \sigma_e^2 \in D_\epsilon} \left\| f(W) - \int g(Q^*; \sigma_e^2) f(Q^*) \Pi(dQ^*) \right\| \leq \epsilon.$$

Note the Frobenius distance between two eigen-matrices

$$\text{dist}(W, Q^*)^2 = 2n - 2\text{tr}(W^{\text{T}} Q^*) = 2 \sum_{j=1}^n (1 - g_{j,j}),$$

where $g_{i,j}$ is the element of $G = W^{\text{T}} Q^*$, where $|g_{j,j}| \leq 1$ due to orthonormality of G . Let $(1 - g_{j,j}) = s_{j,j} \sigma_e$, then $\sum_{j=1}^n (1 - g_{j,j}) = \sum_{j=1}^n s_{j,j} \sigma_e$. As $\sigma_e^2 \rightarrow 0$, $\text{dist}(W, Q^*) \rightarrow 0$ for any fixed $(s_{1,1}, \dots, s_{n,n})$. By the continuity of f and compactness of Stiefel manifold, as $\sigma_e^2 \rightarrow 0$

$$\sup_{W \in \mathcal{V}^*} \left\| f(W) - f(Q^*) \right\| \rightarrow 0. \quad (12)$$

Now

$$\begin{aligned}\Delta &\leq Z^{-1}(\sigma_e^2, D, B) \int \sup_{W \in \mathcal{V}^*} \left\| f(W) - f(Q^*) \right\| \text{etr} \left\{ \frac{1}{2\sigma_e^2} DQ^{*\text{T}} [WBW^{\text{T}}] Q^* \right\} \Pi(dQ^*) \\ &= Z^{-1}(\sigma_e^2, D, B) \int \sup_{W \in \mathcal{V}^*} \left\| f(W) - f(WG) \right\| \text{etr} \left\{ \frac{1}{2\sigma_e^2} DG^{\text{T}} BG \right\} \Pi(dG)\end{aligned}$$

where the second line is due to the invariant volume of rotation via W . It can be verified that

$$\begin{aligned}\text{tr}(DG^{\text{T}} BG) &= \sum_{i=1}^n \sum_{j=1}^n b_i d_j g_{i,j}^2 \\ &= \sum_{j=1}^n b_j d_j - \sum_{j=1}^n b_j d_j (1 - g_{j,j}^2) + \sum_{j=1}^n \sum_{i \neq j} b_i d_j g_{i,j}^2 \\ &\leq \sum_{j=1}^n b_j d_j - \sum_{j=1}^n b_j d_j (1 - g_{j,j}^2) + \sum_{j=1}^n d_j b_n \sum_{i \neq j} g_{i,j}^2 \\ &= \sum_{j=1}^n b_j d_j - \sum_{j=1}^n b_j d_j (1 - g_{j,j}^2) + \sum_{j=1}^n d_j b_n (1 - g_{j,j}^2) \\ &= \sum_{j=1}^n b_j d_j + \sum_{j=1}^n d_j (b_n - b_j) (1 - g_{j,j}^2) \\ &= \sum_{j=1}^n b_n d_j - \sum_{j=1}^n d_j (b_n - b_j) g_{j,j}^2\end{aligned}$$

where the first inequality is due to $d_j \geq 0$ and $b_n \geq b_i$ for all i ; the fourth line is due to the 1 unit norm for each column of G .

Changing variable to $S = \{s_{i,j}\}_{(i,j)}$, with $s_{i,j}\sigma_e = g_{i,j}$

$$\begin{aligned}\Delta &\leq Z^{-1}(\sigma_e^2, D, B) \exp \left[\frac{1}{2\sigma_e^2} \sum_{j=1}^n b_n d_j \right] \int_{\mathcal{S}} \sup_{W \in \mathcal{V}^*} \left\| f(W) - f(WG) \right\| \\ &\quad \times (\sigma_e)^{n^2} \exp \left[-\frac{1}{2\sigma_e^2} \sum_{j=1}^n d_j (b_n - b_j) (1 - s_{j,j}\sigma_e)^2 \right] \Pi(dS)\end{aligned}\tag{13}$$

Again, changing variable $s_{j,j}^* = 1/\sigma_e - s_{j,j}$ and $s_{i,j}^* = s_{i,j}$ for $i \neq j$. Note that its space of S^* is simply \mathcal{V}^*

scaled by $1/\sigma_e$. We have

$$\begin{aligned}
& \int_{\mathcal{S}} (\sigma_e)^{n^2} \exp \left[-\frac{1}{2\sigma_e^2} \sum_{j=1}^n d_j (b_n - b_j) (1 - s_{j,j} \sigma_e)^2 \right] \Pi(dS) \\
&= \int_{\mathcal{S}^*} (\sigma_e)^{n^2} \exp \left[-\frac{1}{2\sigma_e^2} \sum_{j=1}^n d_j (b_n - b_j) \{1 - (1/\sigma_e - s_{j,j}^*) \sigma_e\}^2 \right] \Pi(dS^*) \\
&\leq (\sigma_e)^{n^2} \int_{\mathcal{S}^*} \Pi(dS^*) \\
&= \text{vol}\{\mathcal{V}^*\} \\
&< \infty
\end{aligned}$$

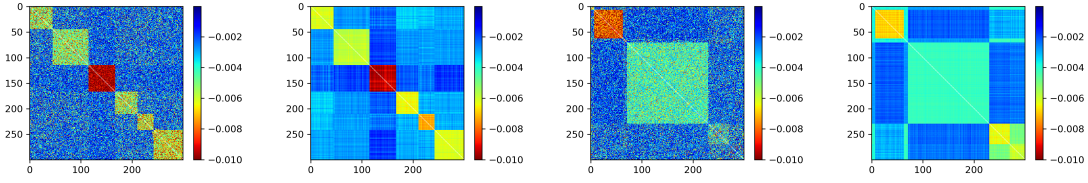
On the other hand, the inverse of the constant in (13)

$$\begin{aligned}
& Z(\sigma_e^2, D, B) \exp \left[-\frac{1}{2\sigma_e^2} \sum_{j=1}^n b_n d_j \right] \\
&= \exp \left[-\frac{1}{2\sigma_e^2} \sum_{j=1}^n b_n d_j \right] \int_{U \in \mathcal{V}^*} \text{etr} \left\{ \frac{1}{2\sigma_e^2} D U^T B U \right\} dU \\
&= \int_{U \in \mathcal{V}^*} \exp \left\{ \frac{1}{2\sigma_e^2} \left(\sum_{i=1}^n \sum_{j=1}^n b_i d_j u_{i,j}^2 - \sum_{j=1}^n b_n d_j \sum_{i=1}^n u_{i,j}^2 \right) \right\} dU \\
&= \int_{U \in \mathcal{V}^*} \exp \left\{ \frac{1}{2\sigma_e^2} \sum_{i=1}^n \sum_{j=1}^n (b_i - b_n) d_j u_{i,j}^2 \right\} dU \\
&= {}_0F_0^{(n)} \left(D^* / (2\sigma_e^2), (B - b_n I_n) \right)
\end{aligned} \tag{14}$$

As $\sigma_e^2 \rightarrow 0$, the last quantity is bounded away from 0 (Koev and Edelman, 2006). Therefore, the constant in (13) is finite as $\sigma_e^2 \rightarrow 0$. Using dominated convergence theorem, when $\sigma_e^2 \rightarrow 0$, $\Delta \rightarrow 0$. This means there is an neighborhood $D_\epsilon = \{\sigma_e^2 : \sigma_e^2 > M_\epsilon\}$, so that $\Delta < \epsilon$. \square

Supplementary Materials

Simulation for Estimating Latent Structure



(a) Laplacian of a simulated graph. (b) Estimated spiked Laplacian. (c) Laplacian of a simulated graph. (d) Estimated spiked Laplacian.

Figure 8: The proposed model correctly finds the latent community structures in 200 simulated graphs.

Additional Components in Working Memory Data Analysis

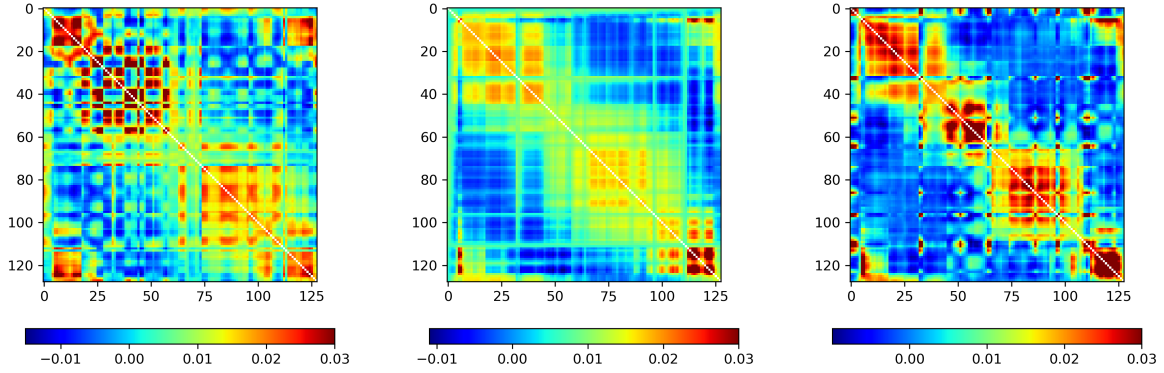


Figure 9: Fitted Laplacian shows the structure underneath the raw connectivity matrix.